Since January 2020 Elsevier has created a COVID-19 resource centre with free information in English and Mandarin on the novel coronavirus COVID-19. The COVID-19 resource centre is hosted on Elsevier Connect, the company's public news and information website.

Elsevier hereby grants permission to make all its COVID-19-related research that is available on the COVID-19 resource centre - including this research content - immediately available in PubMed Central and other publicly funded repositories, such as the WHO COVID database with rights for unrestricted research re-use and analyses in any form or by any means with acknowledgement of the original source. These permissions are granted for free by Elsevier for as long as the COVID-19 resource centre remains active.

Biomaterials 296 (2023) 122071

Contents lists available at ScienceDirect

Biomaterials

journal homepage: www.elsevier.com/locate/biomaterials

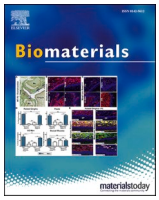

Remote Co-loading of amphipathic acid drugs in neutrophil nanovesicles infilled with cholesterol mitigates lung bacterial infection and inflammation

Jin Gao, Yujie Su, Zhenjia Wang *

Department of Pharmaceutical Sciences, College of Pharmacy and Pharmaceutical Sciences, Washington State University, Spokane, WA, 99202, USA

ARTICLE INFO

Keywords:
Neutrophil nanovesicles
Methyl prednisolone
Azlocillin
Remote loading
Inflammation
Lung infections

ABSTRACT

Lung bacterial infections could result in acute lung inflammation/injury (ALI) that propagates to its severe form, acute respiratory distress syndrome (ADRS) leading to the death. The molecular mechanism of ALI is associated with bacterial invasion and the host inflammation response. Here, we proposed a novel strategy to specifically target both bacteria and inflammatory pathways by co-loading of antibiotics (azlocillin, AZ) and anti-inflammatory agents (methylprednisolone sodium, MPS) in neutrophil nanovesicles. We found that cholesterol infilling in the membrane of nanovesicles can maintain a pH gradient between intra-vesicles and outer-vesicles, so we remotely loaded both AZ and MPS in single nanovesicles. The results showed that loading efficiency of both drugs can achieve more than 30% (w/w), and delivery of both drugs using nanovesicles accelerated bacterial clearance and resolved inflammation responses, thus preventing the potential lung damage due to infections. Our studies show that remote loading of multiple drugs in neutrophil nanovesicles which specifically target the infectious lung could be translational to treat ARDS.

1. Introduction

Pseudomonas aeruginosa (*P. aeruginosa*) is a Gram-negative bacterium that invades into the body leading to infectious diseases [1–3]. Since there is the natural resistance to antibiotics and the ability to form biofilms, understanding of metabolism of pathogens and developing vaccines are the major focus to treat infections [4,5]. *P. aeruginosa* is common to infect the lung. The lung infection causes the life threatening to patients with comorbidities [6] because it leads to a severe lung inflammation response [7]. Although the inflammation response is a protection effect, it results in acute lung inflammation/injury (ALI) if the inflammation is overwhelming and out of control. ALI may quickly propagate to acute respiratory distress syndrome (ARDS) and its mortality is 30–50% [8–11]. To treat bacterial infections, high dose antibiotics are administered to patients for life saving, but this could induce the systemic toxicity [12,13]. Under the high dose and frequencies of administering antibiotics, pathogens are gradually resistant to the treatment [13,14]. It is critical to develop new delivery systems to concentrate drugs in infectious sites, thus possibly avoiding the antimicrobial resistance [15–17].

In lung infections, lipopolysaccharide (LPS) derived from *P. aeruginosa* causes a host inflammation response. The inflammation induces neutrophils activated, and subsequently neutrophils bind to and transmigrate across activated endothelium in the lung to restrain the spreading of pathogens. Therefore, it has been proposed that neutrophil membrane-formed nanovesicles can home the infectious lesions in the lung and deliver therapeutics to treat lung infections [18–22]. However, the biomedical applications of nanovesicle-based delivery systems are limited by the low drug loading into nanovesicles. Polymeric nanoparticles have the high drug loading, so it was proposed to load polymeric nanoparticles inside cell-membrane derived nanovesicles [15, 23–25], but it is unknown how effective this loading of NPs is inside nanovesicles.

Cell membrane-derived nanovesicles are made of a lipid bilayer like liposomes, and it was first proposed to remotely load piceatannol (weak acid) inside nanovesicles via a pH gradient [20]. To maintain the pH gradient, cholesterol was added to nanovesicle suspensions [26]. In their studies, chloroform was used to dissolve cholesterol. However, this caused nanovesicle aggregation and denature targeted ligands on membrane of nanovesicles. As the remote loading represents one of most effective means of liposomal drug encapsulation [27–29] , the application to neutrophil nanovesicles would open new opportunities for

* Corresponding author.
E-mail address: zhenjia.wang@wsu.edu (Z. Wang).

https://doi.org/10.1016/j.biomaterials.2023.122071
Received 1 November 2022; Received in revised form 7 February 2023; Accepted 28 February 2023
Available online 28 February 2023
0142-9612/© 2023 Elsevier Ltd. All rights reserved.

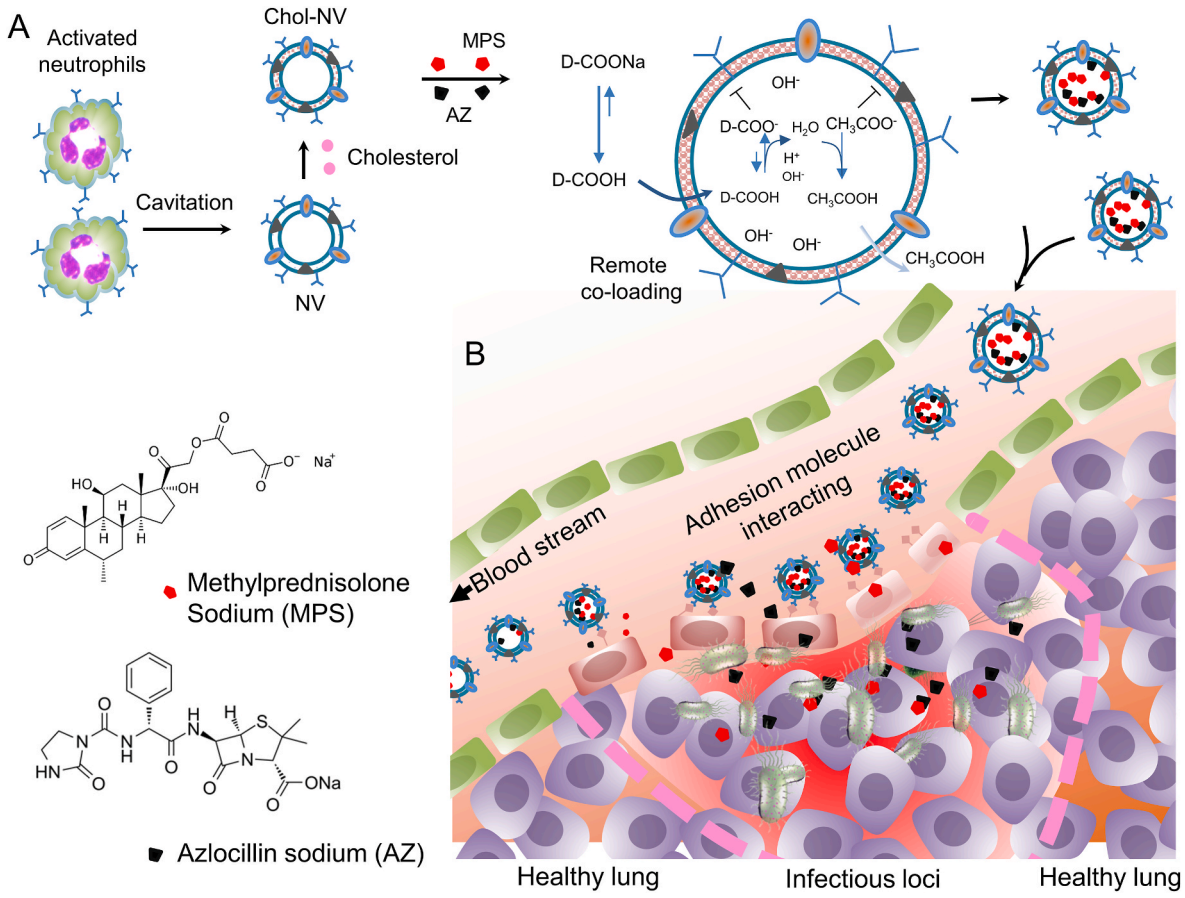

Fig. 1. Schematic illustration for the simultaneous delivery of an anti-inflammatory agent and an antibiotic to the infectious site in the lung. (A) Activated neutrophils (HL-60 cells) are subjected to a cavitation force to produce cell membrane-derived nanovesicles. The nanovesicle membrane is infilled with cholesterol to maintain the pH gradient between intra-vesicles and outer-vesicles, so MPS and AZ can penetrate the membrane when D-COOH (D represents MPS or AZ) is neutral. After D-COOH is inside vesicles, DCOOH is deprotonated to become D-COO$^-$ and then it is entrapped inside vesicles. (B) In a lung infection mouse model, neutrophil nanovesicles will home to infectious sites when they are intravenously administered to the mice because the nanovesicles inherit the targeting adhesion molecules of neutrophils. Therefore, effectively delivering MPS and AZ to the lung mitigates inflammation responses and clears bacteria. NV denotes neutrophil membrane-formed vesicle. Chol denotes cholesterol.

developing the next generation of nanotherapeutics. Since the lung infection is involved with bacterial invasion and the host inflammation response induced by bacteria, the rapid removal of bacteria in the lung and restoration of the host homeostasis are critical to develop therapies for treating lung infections. Methylprednisolone sodium succinate is clinically used anti-inflammatory agent [30,31], and azlocillin (AZ) [32,33] is an acylampicillin antibiotic for treating infections by *P. aeruginosa*. Effective delivery of both drugs into the infectious lung could increase the therapeutic outcome in lung infections and avoid the systemic side effect.

Here, we designed the co-loading of MPS and AZ inside single neutrophil nanovesicles via the pH gradient and found that cholesterol dissolved in pyridine can be efficient to infill in the membrane of neutrophil nanovesicles to maintain the pH gradient between intra-vesicles and outer-vesicles. In addition, embedded cholesterol did not change the membrane integrity of nanovesicles and their cellular targeting to the lung vasculature. In the mouse lung model of *P. aeruginosa* infection, nanovesicles co-loaded with MPS and AZ cleared bacteria and decreased the cytokine storm in the blood and lung. Furthermore, the nanovesicles prevented the lung injury from edema and alleviated neutrophil infiltration to the lung. The results demonstrate that remote loading of multiple drugs to biomimetic nanovesicles represents the potential translation in treating a wide range of diseases including cancer. Fig. 1 shows the design of co-loading of multiple drugs to nanovesicles and the hypothesis that delivering both an anti-inflammatory agent and an antibiotic to the infectious site in the lung enhances the therapies to lung infectious diseases.

2. Materials and methods

2.1. Chemicals and reagents

Acetate sodium (NaAc), cholesterol (Chol), pyridine, dimethyl sulfoxide (DMSO) and other important chemicals prepared for buffers were purchased from Sigma-Aldrich (St. Louis, MO). The antibodies, such as *anti*-integrin β2, *anti*-integrin α4, PSGL-1, *anti*-PECAM-1, *anti*-αV, *anti*-TLR4 anti- Intercellular adhesion molecule-1 (ICAM-1) and anti-Glyceraldehyde-3-phosphate dehydrogenase (GAPDH), were bought from Santa Cruz Biotechnology (Sanit Cruz, CA). The reagents for cell culture were obtained from Lonza (Walkersville, MD) and Life Technologies (Grand Island, NY).

2.2. Cell culture

Human myeloid leukemia HL60 cells were grown in a RPMI 1640 medium (Lonza, Walkersville, MD) supplemented with 10% fetal bovine serum (Cat. No. S11550H, Atlanta, Flowery Branch, GA) and 1% Pen-Strep solution (Cat. No. 15140–122, life Technologies, Grand Island, NY). All cells were cultured at 37 °C in a humidified atmosphere with 5% CO_2. Human umbilical vein endothelial cells (HUVECs, Lonza,

Walkersville, MD) were cultured in EBM medium, supplemented with a culture kit (Lonza, Walkersville, MD), and used within passage seven in all experiments. All cells were cultured at 37 °C in a humidified atmosphere with 5% CO_2.

2.3. Vesicle preparation and characterization

HL60 cells were induced to differentiate by culturing in the presence of 1.25% DMSO (D4540, Sigma-Aldrich, St. Louis, MO) for 4 days. The mature cells were then collected and suspended at 10^7/ml in 250 mM NaAc at pH 8.8, and the cells were subjected to nitrogen cavitation twice under 500 psi, 20 min each time [18]. The cavitated suspension was centrifuged at 2000 g and then the supernatant was centrifuged at 100 000 g for 30 min. The vesicles in pellets were washed once with 250 mM NaAc at pH 8.8. The prepared vesicles were incubated with 10% weight of cholesterol dissolved in pyridine at 37 °C for 60 min. The prepared vesicles were analyzed to measure their size and zeta potential using dynamic light scattering on a ZS90 nano sizer (Malvern, Malvern, UK).

2.4. Measurement of pH inside nanovesicles

To measure the inner pH values of NVs, a pH sensor, SNARF-1 carboxylic acid (Cat. No. S23920, Waltham, MA) at 3 μM was added into the cell suspension buffer, and then NVs were produced by nitrogen cavitation [5,18,34]. Next, 2%, 5%, 10%, 15% (ratio (w/w) of Chol and NV) or no cholesterol were added to the suspension. After incubation at 37 °C for 30 min, the pH sensor contained NVs were purified as shown in section 2.3. The pH-sensor contained NVs were resuspended in PBS (pH7.4) and the emission fluorescence intensity was measured at 590 nm and 640 nm excited at 488 nm. To calculate pH values, we obtained the standard curve by measuring the emission intensity of free SNARF-1 in different pH buffers in the presence of 10% FBS. The pH values in the NVs were calculated based on the ratio of emission at 590 nm and 640 nm. To evaluate the membrane permeability, the inner pH values at 0, 30, 60, 90, 120 min post-resuspending were measured. To verify cholesterol increased the drug encapsulation, we used fluorescein sodium as a model drug. Fluorescein sodium at 5 μg/ml was added into the resuspending buffer before nitrogen cavitation to produce NVs. After the NV preparation, the fluorescent intensity at 515 nm was measured.

2.5. Characterization of NVs

Cholesterol in vesicles was measured using a cholesterol fluorometric assay kit purchased from Cayman chemicals (Cat. No. 10007640, Ann arbor, MI USA) and the measurement was performed following the manufacturer's guideline. Protein contents were measured by a bicinchoninic acid (BCA, Cat. No. 23228, Rockford, IL) kit. The vesicle surface proteins were detected using western blotting. The samples (20 μg total proteins) were separated on SDS-PAGE and transferred to PVDF membranes. The membranes were then blotted with specific antibodies for each protein. Antibodies, such as *anti*-integrin β2 (Cat. No. 393790, clone C-4), *anti*-integrin α4 (Cat. No. 365569, clone C-2), PSGL-1 (Cat. No. 13535, clone KPL1), *anti*-PECAM-1(Cat. No. 376764, clone H-3) *anti*-αV (Cat. No. 376156, clone H-2), *anti*-TLR4 (Cat. No. 293074, clone 25) were purchased from Santa Cruz Biotechnology (Santa Cruz, CA). Sheep *anti*-hCD47 polyclonal antibodies were obtained from R&D systems Inc (Cat. No. AF4670-SP, Minneapolis, MN). Next, the HRP-conjugated goat anti-mouse antibody (Cat. No. 2005) or donkey anti-sheep antibody (Cat. No. 2473, Santa Cruz, CA) was incubated following addition of West Femto Maximum Sensitivity Substrate (Cat. No. 34095, Thermo Scientific, Rockford, IL) for Western blot quantification.

2.6. Cryo-TEM imaging

Cryo-TEM images were taken by a TF20 transmission electrical microscope, equipped with a liquid nitrogen stage (FEI, Hillsboro, OR). To make the sample, a drop of NVs solution (1 mg/ml) was deposited on a carbon-coated grid. The grid was quickly dropped in liquid nitrogen and stored over-night after soaked with filter paper [18].

2.7. Drug loading

After the prepared vesicles were infilled with cholesterol at 10% (w/w), drug loading was conducted by incubating Chol-NVs with MPS (Cat. No. B4953, Apexbio technology LLC, Houston, TX) and/or AZ (Cat. No. J66895, Thermo Fisher Scientific, Ward Hill, MA) with different drug inputs at 37 °C for 1 h. The drug-loaded NVs were purified using a 5% glucose pre-equalized PD Minitrap Sephadex G25 column (Cat. No. 28922530, GE healthcare, Buckinghamshire, UK) to remove free drugs. The loaded drug was measured by high performance liquid chromatography (HPLC) after the drug-loaded NVs were extracted with ethanol at 9-fold volume. The loading yield was calculated as the mass of drug divided by the total mass of vesicles. The encapsulation efficiency was calculated as the mass of drug divided by the total mass of the drug input.

2.8. Drug release profiling

The drug release profiles of the formulations were measured using Slide-A-Lyzer G2 dialysis devices with a molecular weight cut-off of 20 kDa (Cat. No. G235033, Spectrum Laboratories, Rancho Dominguez, CA). MPS and/or AZ-loaded vesicles were dialyzed against 50-fold volume of PBS pH 7.2 at 37 °C.

2.9. MPS and AZ measurement by HPLC

Measurement of MPS and AZ was performed using HPLC on a Waters 2690 module with an ultraviolet detector. The same mobile phase including acetonitrile and sodium hydrate-adjusted 0.1 M acid acetate buffer (pH5.7) was used. The mobile phase ratio for MPS was set at 32:68, and for AZ, 20:80 was used, respectively. The flow speed was set at 0.9 ml/min and the wavelengths were set at 250 nm and 209 nm, respectively. The chromatography was conducted on a 250 mm × 4.6 mm Restek Ultra C18 5 μm column (Bellefonte, PA). The drug-loaded formulations were diluted with 9-fold ethanol to extract the drug before loading for analysis.

2.10. HUVEC binding of Chol-NVs in vitro

HUVECs (6-well plates) were treated with 50 ng/ml TNF-α (carrier free, Santa Cruz, CA) for 4 h. The activated HUVECs were then harvested and incubated with 2 and 20 μg/ml vesicles, pre-stained by lipophilic tracer benzoxazolium, 3-octadecyl-2-[3-(3-octadecyl-2(3H)-benzoxazolylidene)-1-propenyl]-, perchlorate (DiO, Cat. No. V22889, Invitrogen, Waltham, MA), with or without additional cholesterol) at 37 °C for 30 min. The cells were then analyzed for fluorescent intensity by Gallios flow cytometer (Beckman coulter, Brea, CA).

2.11. In vivo visualizing adhesion of Chol-NVs on endothelium

All experiments using animal models were approved by the Institutional Animal Care and Use Committee of Washington State University, Pullman, USA. CD-1 male mice were purchased from Envigo (Denver, CO). 3 h after *i. p.* LPS challenging, 3 μg Alexa 647 labelled anti-CD31 and 30 μg DiO-stained Chol-NVs, were *i. v.* Administered to mice via a tail vein. The mice were then anesthetized with ketamine (100 mg/kg) and xylazine (5 mg/kg) via *i. p.* Injection, and the cremaster tissue was exposed on an intravital microscopy tray [18,35]. The vasculature was imaged using our intravital microscope (A1R+, Nikon, Tokyo, Japan). The cremaster tissue was perfused with bicarbonate-buffered saline through the imaging period.

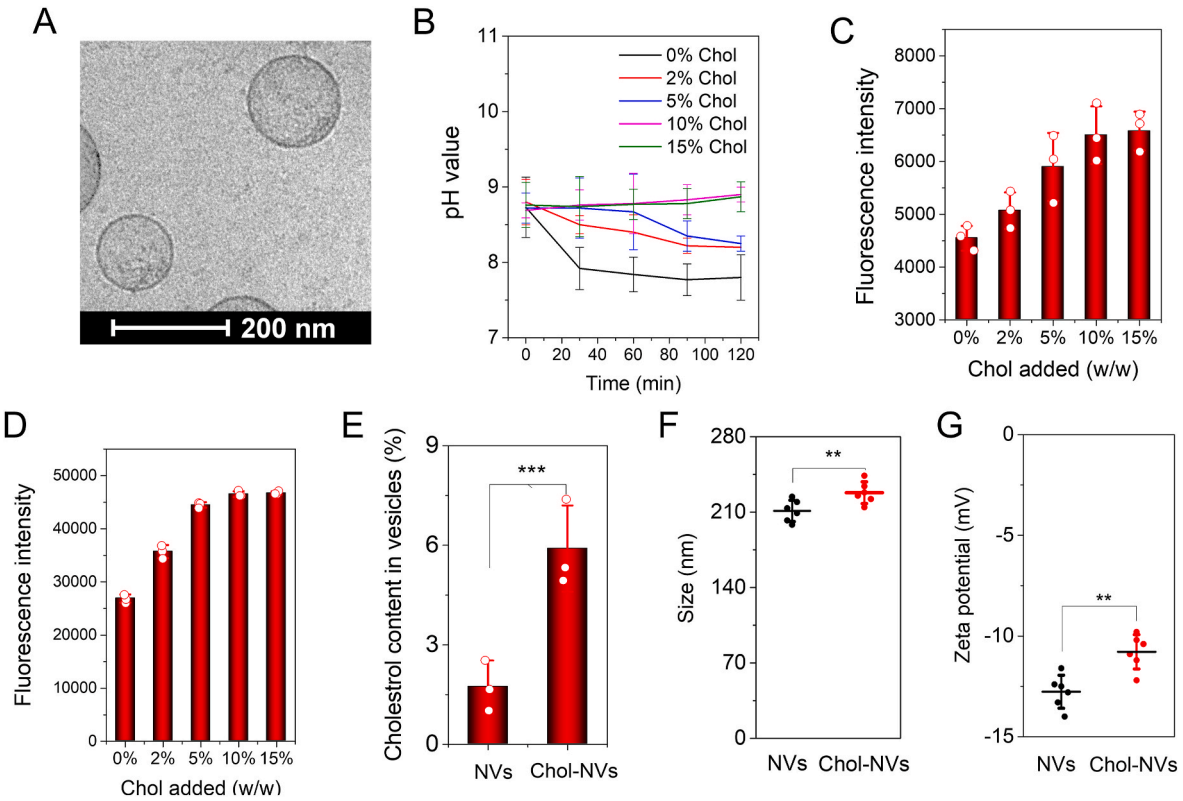

Fig. 2. Infilling of cholesterol decreases the membrane permeability of NVs to establish a pH gradient between intra-vesicles and outer-vesicles. (A) Cryo-TEM image of NVs. (B) pH values in NVs measured using a pH indicator of SNARF-1 entrapped inside NVs and NVs were suspended in PBS at pH7.4; (C) Fluorescent intensity of SNARF-1 contained in NVs after the incorporation of cholesterol to NVs; (D) Fluorescent intensity of fluorescein sodium contained in NVs after the incorporation of cholesterol to NVs; (E) Cholesterol percentages in NVs determined using a cholesterol fluorometric assay kit; (F) Sizes of NVs with or without addition of cholesterol; (G) Zeta potentials of NVs with or without addition of cholesterol; In E, F and G, 10% (w/w) cholesterol was supplemented. Data presented as the mean ± SD, n = 3, 6. **P < 0.01, ***P < 0.001.

2.12. Biodistribution of NVs

NVs were stained with DiD at 0.2% (w/w) at 37 °C for 30 min. The lung inflammation mouse model was generated by intratracheal administration of 15 mg/kg LPS. At 3 h after LPS challenge, 0.5 mg NVs were intravenously given to inflammatory or healthy mice respectively. The blood was collected in a tube with heparin as anticoagulant via facial vein. The mice were then euthanized, and major organs (heart, liver, spleen, kidney, and lung) were excised. The tissue was then homogenized and the suspension was centrifugated to obtain the supernatants. The DiD contents in supernatants were measured at 640ex/660em using a plate reader to quantify the biodistribution of NVs.

2.13. Anti-inflammatory efficacy of Chol-NVs in vitro

HUVECs were passaged and seeded on a 24-well plate with 2×10^5 cells per well one day prior to the experiment. The cells were activated using 50 ng/ml TNF-α for 5 or 10 h in the presence or absence of 100 μg/ml MPS in the forms of free or MPS-NVs. Then, the cells were lysed with 100 μl cell lysis buffer respectively and subjected for western blotting to detect the ICAM-1 expression using monoclonal *anti*-ICAM-1 antibody (Cat. No. 390483, clone H-4) normalized to *anti*-GAPDH (Cat. No. 365062, clone G-9, Santa Cruz, CA).

2.14. Anti-inflammatory efficacy of Chol-NVs in vivo

For the *in vivo* anti-inflammation efficacy evaluation, a dose of 15 mg/kg LPS (*Escherichia coli* 0111:B4, Sigma-Aldrich, St. Louis, MO) was intratracheally administered to CD-1 mice with a high pressure aerosolizer (Penn-century Inc, Wyndmoor, PA) [19]. 2 h later, the mice intravenously received buffer, free MPS and MPS-MVs. The lung bronchoalveolar lavage fluids were collected by washing the lung three times with 0.9 ml HBSS each time. The total cells were obtained by centrifugation at 420*g* for 5 min and neutrophil percentages were determined by flow cytometry after the cells were stained with Alexa 488 conjugated *anti*-Ly-6G antibody (clone 1A8, Santa Cruz, CA). Cytokine levels and protein contents were measured using ELISA kits (San Diego, CA) and BCA method (Rockford, IL) respectively.

2.15. Antimicrobial efficacy in vitro

To measure *in vitro* antimicrobial efficacy of AZ-loaded NVs, 1×10^6 CFU/ml *P. aeruginosa* was incubated in LB on a 96-well plate with 5% glucose, free AZ, and AZ-Vesicles for 16 h respectively. The bacterial growth was determined by measuring the optical density at 600 nm (OD_{600}). The half maximal inhibitive concentrations (IC_{50}) were then calculated with Prism GraphPad 6.0. The killing capability of AZ-loaded NVs was determined by incubating 10^6 CFU bacteria with 5% glucose, free AZ, and AZ-Vesicles for 20 min. The bacteria were then serially diluted and spread on LB plates to culture at 37 °C overnight. The CFU on the plates were counted to evaluate the bacteria-killing efficacy.

2.16. Antimicrobial efficacy assay in vivo

In the lung infection model, CD-1 mice were intratracheally given 5×10^5 CFU of *P. aeruginosa* per animal. 4 h later, the animals were grouped and *i. v.* Given drugs in different formulations, and at the indicated time points, the animals were anesthetized with *i. p.* Injection of ketamine and xylazine mixture. The trachea was cannulated, and 1 ml of HBSS was intratracheally infused and withdrawn to obtain lavage

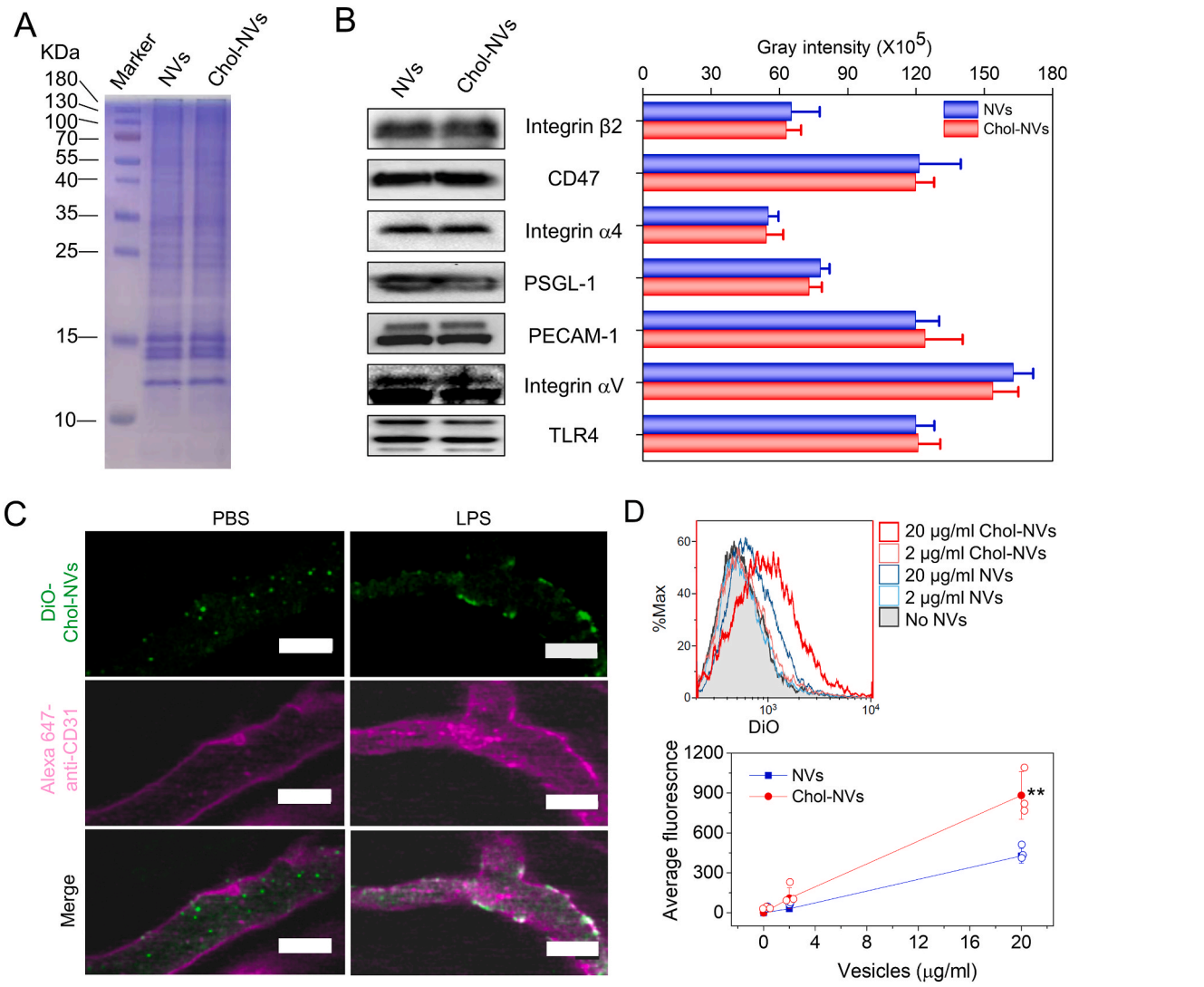

Fig. 3. Infilling of cholesterol to NVs does not impair the binding/uptake of NVs by activated endothelium. (A) Protein profiles of NVs and Chol-NVs. (B) Intercellular adhesion molecules on NVs measured by Western blot and their quantification. (C) The binding of Chol-NVs to activated vasculature determined by intravital microscopy of cremaster tissues of the live mouse. 3 h after intraperitoneal injection of LPS at 15 mg/kg, Chol-NVs were *i. v.* Injected and the live cremaster tissue was imaged using intravital microscope. The control is that the mouse was treated with PBS. Scale bar, 50 μm. (D) Uptake of DiO-Chol-NVs and DiO-NVs in HUVECs detected by flow cytometry and the quantification of their uptake. Scale bar = 100 μm. Data are presented as the mean ± SD, n = 3. Comparison was performed by one side Student's *t*-Test and * *P < 0.01.

fluid. This procedure was repeated twice more. The lung lavage fluids were spread on LB plates to measure CFU. The remaining lavage fluids were then centrifuged at 420 g for 10 min and the supernatants were removed to measure cytokine levels. The pelleted cells were suspended in PBS to count the total cell number with a hematocytometer. To measure the percentage of the neutrophils, Alexa Fluor 488 conjugated anti-mouse Ly-6G antibody (clone 1A8, Santa Cruz, CA) were used and then the stained cells were analyzed on flow cytometry.

2.17. Statistics

The differences among groups were evaluated using one-way ANOVA and were considered significant and extremely significant when $P \leq 0.05$ and $P \leq 0.01$, respectively. The IC_{50} were obtained by sigmoidal fitting with Prism GraphPad 6.0.

3. Results and discussion

3.1. Infilling cholesterol in nanovesicle membrane decreases membrane permeability to establish a pH gradient

We produced neutrophil membrane nanovesicles (NVs) following the similar method [18,20], and the TEM image (Fig. 2A) shows that NVs are made of membrane structures like liposomes. Cholesterol is one of the major sterol component of animal cell membranes making up to 30% of the lipid bilayer and the amount is dependent on cell types [36]. Cholesterol can immobilize the lipid layer of membrane, thus reducing the membrane fluidity. Furthermore, the cholesterol amount in the cell membrane effects on the permeability of ionic molecules across the membrane [37,38]. We hypothesized that incorporating cholesterol in the membrane of neutrophil nanovesicles may establish a pH gradient between intra-vesicles and outer vesicles for remote drug loading. In the experiments, we observed that using chloroform as the solvent to dissolve cholesterol caused the aggregation of nanovesicles. We found that dissolving of cholesterol in pyridine did not cause the nanovesicle

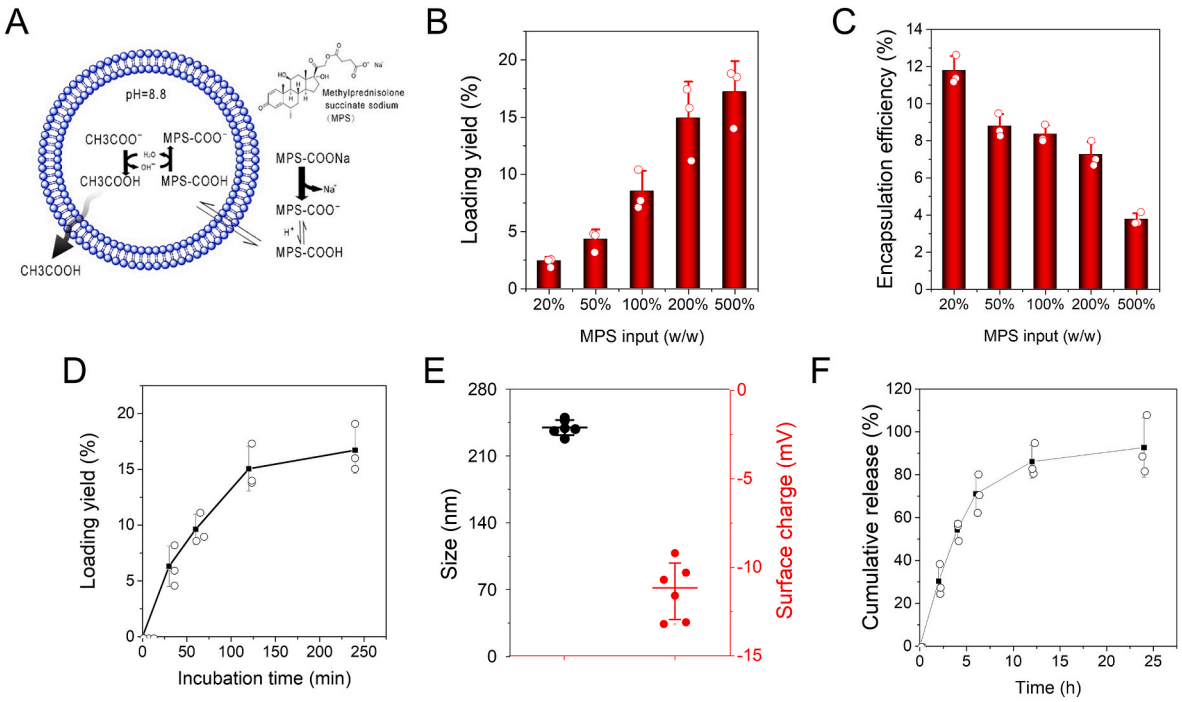

Fig. 4. Remote loading of MPS in Chol-NVs and controlled release of MPS. (A) Schematic illustration for the remote loading of MPS inside NVs via a pH gradient. (B) Remote loading efficiencies of MPS in Chol-NVs is dependent on MPS input. The loading yield calculated by the amount of MPS divided by the mass of Chol-NVs. (C) Encapsulation efficiencies of MPS in Chol-NVs is dependent on MPS input. (D) The loading efficiency of MPS over incubation times. (E) Size and zeta potential of MPS-loaded Chol-NVs at what loading efficiency of MPS. (F) The release profile of MPS from MPS-Chol-NVs at what loading efficiency of MPS. Data presented as the mean ± SD, n = 3,6.

aggregation and we were able to add 15% (w/w) cholesterol to the nanovesicle suspension.

We first tested our hypothesis that infilling of cholesterol into the membrane of nanovesicles will maintain the pH inside nanovesicles. To do that, we supplemented a pH sensor SNARF-1 inside nanovesicles during the production of NVs and then we added the different amount of cholesterol into the suspension of NVs. The pH inside nanovesicles was 8.8 and the external medium had the pH of 7.4. Fig. 2B shows that nanovesicles rapidly decreased the pH values from 8.8 to 7.4 without addition of cholesterol, indicating that there was the same pH in intra-vesicles and external medium. However, when we increased cholesterol to the suspension of NVs, we observed that NVs became to maintain the original pH at 8.8 and beyond 10% cholesterol added to NVs, the pH values were stable in NVs. The results indicate that infilling of cholesterol to NVs decreased the membrane permeability, thus producing a pH gradient between the intra-vesicles and outer-vesicles. Furthermore, we measured the fluorescent intensities of SNARF-1 and found that the fluorescent intensities increased with adding of cholesterol to NVs, and it saturated after the addition of cholesterol beyond 10% cholesterol (Fig. 2C). This is consistent with the result in Fig. 2B. To further verify this observation, we added a fluorescent dye of fluorescein sodium (a model drug) inside NVs, and we measured its fluorescent intensities (Fig. 2D). We observed the same trend as in Fig. 2C.

To determine whether cholesterol was infilled into the membrane of NVs, we quantitatively measured the cholesterol contents after we isolated NVs. We found that NVs possessed 1.7% before adding exogeneous cholesterol. However, 5.9% cholesterol was in NVs when 10% (w/w) cholesterol was added to the suspension of NVs (Fig. 2E), and incorporation efficiency of cholesterol to the membrane of NVs was 42%. We also measured the size (Fig. 2F) and zeta potential of NVs (Fig. 2G) and we found that the size and zeta potential of NVs increased from 211.2 nm to 228.0 nm, and from −12.8 mV to −11.1 mV, respectively. The increase in size and zeta potential further supports that cholesterol was infilled in NVs.

3.2. *Cholesterol infilling to NVs does not affect the targeting ability of NVs*

The previous studies have shown that the presence of cholesterol impacted on the membrane proteins [39] and the intermolecular interactions [40]. To verify whether infilling of cholesterol to the membrane of NVs effects on the targeting capability of NVs to activated vasculature, we studied the protein profile on NVs and found that there was no difference of major proteins after we embedded cholesterol into the membrane of NVs (Cholesterol infilled to NVs is referred as Chol-NVs) (Fig. 3A). Furthermore, we quantitatively analyzed major cellular adhesion proteins on NVs using western blotting and found that adding of cholesterol did not change the amount of these cellular adhesion proteins (Fig. 3B). We also compared these adhesion proteins on Chol-NVs with those on their parent cells (HL 60 cells). It was shown that GAPDH, a cytosol protein were significantly reduced in Chol-NVs (Fig. S1), indicating that Chol-NVs are mainly made from the source cell membrane, which is consistent with our previous studies [19–21].

Next, we established intravital microscopy to visualize whether Chol-NVs can still bind to activated vasculature [41–43]. We exposed the cremaster tissue to allow us to image blood circulation after the mouse was challenged with LPS to produce systemic inflammation [35, 44]. Without LPS treatment to the mouse, we observed that Chol-NVs circulated in the bloodstream and never attached to the vasculature (Fig. 3C). In contrast, Chol-NVs bound to the vasculature when the mouse was treated with LPS, and we did not observe the detachment of Chol-NVs during imaging (Fig. 3C). Moreover, we studied the biodistribution of NVs after intravenous injection in acute lung inflammation mouse model and we found that NVs significantly accumulated in the inflammatory lungs compared to the healthy lung (Fig. S2). The results indicated that Chol-NVs may be internalized in vascular endothelium. To confirm the targeting ability *in vivo*, we performed the *in vitro* studies on uptake of NVs by endothelial cells (HUVECs). Fig. 3D is the flow cytometry results, showing that the cellular uptake of NVs increased with the concentrations of NVs, and adding of cholesterol to

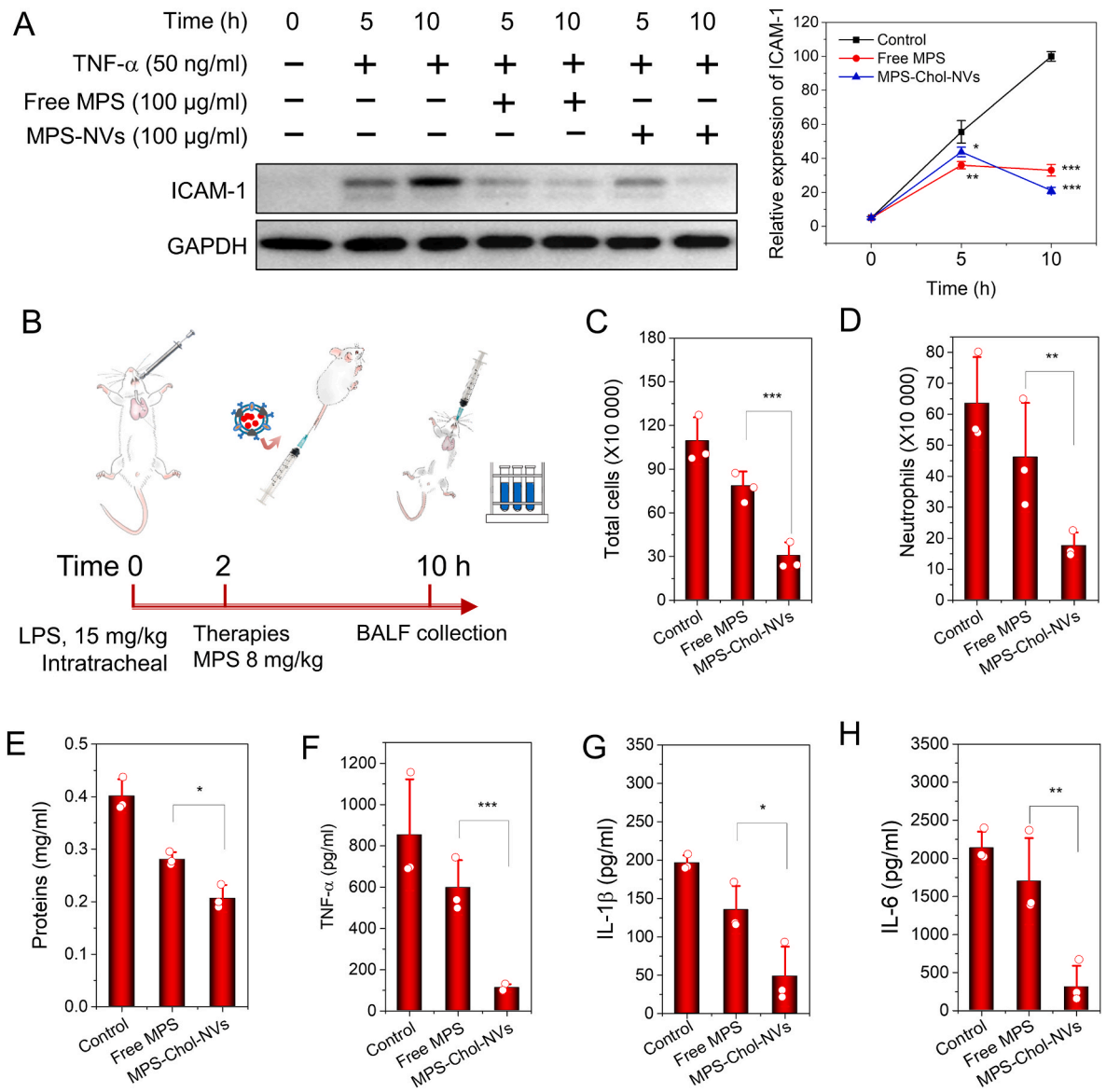

Fig. 5. MPS-loaded Chol-NVs regulates endothelium to alleviate the lung inflammation. (A) MPS-loaded Chol-NVs inhibit the ICAM-1 expression of HUVECs challenged by TNF-α (50 ng/ml) and their quantification. (B) The protocol for lung inflammation of the mouse model. MPS-loaded Chol-NVs mitigate the lung inflammation responses. Total cells (C), neutrophils (D), total proteins (E), TNF-α (F), IL-1β (G), IL-6 (H) in BALF. Data presented as the mean ± SD, n = 3. *P < 0.05, **P < 0.01, ***P < 0.001.

NVs did not affect the cellular uptake. However, it is interesting to observe that addition of cholesterol to NVs enhanced the cellular uptake compared to NVs (Fig. 3D). This may be associated with membrane rigidity of NVs [45,46] to increase binding of intercellular adhesion molecules of NVs to endothelial cells. This is consistent with the studies that addition of cholesterol to neutrophils increased the binding of neutrophils to activated endothelium [47].

3.3. Remote loading of MPS in Chol-infilled NVs

Methylprednisolone (MP) is a synthetic steroid and potent by a five-fold of the endogenous glucocorticoid hydrocortisone. It has been used to treat a wide range of inflammatory diseases including endocrine diseases, severe allergies, ulcerative colitis, multiple sclerosis, rheumatoid arthritis and osteoarthritis [48]. Due to the low water solubility of MP, MP is converted to methylprednisolone sodium (MPS) that is a water-soluble esterified prodrug of MP. MPS is a weak amphipathic acid, so MPS may be remotely loaded inside Chol-NVs via a pH gradient (Fig. 4A). To do so, we established a pH gradient where there was pH at 8.8 inside Chol-NVs and pH at 7.4 outside of Chol-NVs. Then we measured the loading of MPS in NVs and we found that we can achieve 15–17% (w/w) of MPS in NVs (Fig. 4B, Fig. S3). We also found that the encapsulation efficiencies decreased with increased MPS input (Fig. 4C). We also studied how incubation time of MPS with NVs effected on the drug loading efficiencies. It is shown that the loading yields reached to the peak 2 h after the incubation of MPS with NVs (Fig. 4D). In addition, we measured the size of Chol-NVs after loading of MPS and found that the size of NVs increased to 239.7 nm compared to Chol-NVs. The zetapotential did not change after loading of MPS (Fig. 4E). When MPS was loaded inside Chol-NVs, the release of MPS was slow and MPS was able to release for 24 h (Fig. 4F). The results indicate that we have successfully loaded MPS inside Chol-NVs via pH gradient.

3.4. MPS loaded Chol-infilled NVs alleviate lung inflammation

We examined whether MPS-loaded Chol-NVs inhibited the

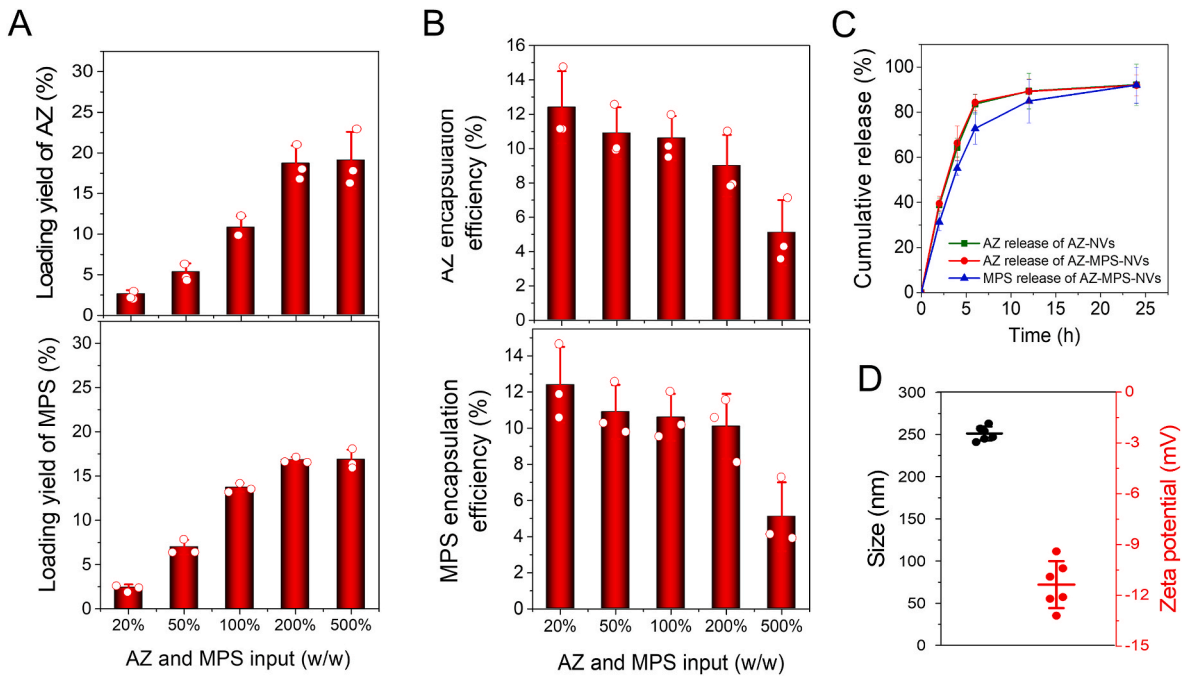

Fig. 6. Co-loading of AZ and MPS into single Chol-NVs. Co-loading efficiency (A) and encapsulation efficiency (B) of AZ and MPS and encapsulation efficiency in Chol-NVs. (C) Release profiles of AZ and MPS of co-loading of AZ and MPS in Chol-NVs. (D) Size and surface charge of AZ-MPS-Chol-NVs. Data presented as the mean ± SD, n = 3.

inflammation response in endothelial cells like free MPS [49,50] because we have shown that NVs specifically targeted activated endothelium during inflammation as shown in Fig. 3. ICAM-1 is a marker of inflammation response after endothelium was treated with TNF-a [51, 52]. HUVECs were treated with TNF-a at 50 ng/ml and simultaneously MPS or MPS-loaded Chol-NVs was added in the culture media. We studied the time course of ICAM-1 expression using Western blot (Fig. 5A), and we found ICAM-1 expression was decreased after the treatment with MPS or MPS-loaded Chol-NVs. We also quantified the Western blot, and we observed that MPS-loaded Chol-NVs had the similar anti-inflammatory effect to free PMS. This result indicates that MPS can be released from NVs, which is consistent with the release result as shown in Fig. 4F.

Next, we tested the therapeutical effect of MPS-Chol-NVs in acute lung inflammation (ALI) [41,53]. We established ALI mouse model via intratracheal spray of liposaccharide (LPS) at 15 mg/ml (Fig. 5B) and administered therapeutics 2 h after LPS. 8 h later, we collected the bronchoalveolar lavage fluid (BALF) to evaluate the therapeutic outcome. We found that cytokines, infiltrated cells and total proteins in BALFs dramatically increased, but these parameters were undetectable in healthy mice. We observed that MPS-loaded NVs dramatically decreased leukocyte infiltration in the lung (Fig. 5C), and in particular, neutrophils contributed to this decrease (Fig. 5D). The results indicated that the loading of MPS in NVs enhanced inflammation resolution. Furthermore, lung vasculature permeability is a marker of lung injury after the inflammation response to LPS. The result showed that total proteins in BALF declined compared to the treatment of free MPS or the disease model (Fig. 5E), indicating that MPS-loaded NVs accelerated inflammation resolution to protect the lung damage. Meanwhile, the cytokines, such as TNF-α (Fig. 5F), IL-1β (Fig. 5G) and IL-6 (Fig. 5H), also decreased accordingly. Collectively, the results demonstrate that loading of MPS in NVs increased the delivery efficiency of MPS to the inflammatory lung tissue, thus accelerating lung inflammation resolution to prevent lung tissue damage.

3.5. Co-loading of MPS and AZ in Chol-infilled NVs

P. aeruginosa is Gram-negative bacteria and a common pathogen to invade in the lung, leading to ALI and ARDS [6]. Antibiotics are clinically used to treat bacterial infections. Azlocillin (AZ) is an acylampicillin antibiotic and highly potent to treat a broad range of bacteria including *P. aeruginosa* [54]. To effectively treat bacterial lung infections, it is needed to deliver therapeutics in the infectious tissues to simultaneously control the host inflammation response and to eliminate bacteria. However, anti-inflammatory agents and antibiotics do not have the ability to target the infectious lesions in the lung.

Here, we asked whether we can co-load AZ and MPS inside single NVs using remote loading approach as shown in Fig. 2. Using the similar approach, we added both AZ and MPS to the suspension of Chol-NVs and measured the loading of AZ and MPS inside NVs using HPLC. The results showed that the drug loading of AZ and MPS can reach up to 19.1% (w/w) and 15.3% (w/w), respectively (Fig. 6A, Figs. S3 and S4), and the total drug loading efficiency in NVs was more than 30% (w/w). However, the encapsulation efficiencies were declined when the input of drugs was increased (Fig. 6B). We also measured the drug release of AZ and MPS co-loaded in NVs and found that their release trends were similar to that of single drug loaded in NVs (such as AZ-loaded in NVs). The drug release was controlled for 24 h (Fig. 6C). The size of AZ and MPS-coloaded in NVs was increased to about 250 nm compared to pure NVs. The zeta potential did not change, and it was around −11.4 mV (Fig. 6D). To test the *anti-P. aeruginosa* potency of AZ-MPS-NVs, we conducted an *in vitro* bacterial killing assay, and found AZ-MPS-NVs exerted the bacterial inhibition capability (Fig. S5A). The IC_{50} of AZ-MPS-NVs was determined to be 1.8 μg/ml, statistically significant less than that of free AZ (Fig. S5B), indicating the carrier can enhance the anti-microbial potency of antibiotics, possibly via enhancing the uptake of the antibiotics by microbes.

3.6. Co-loading of AZ and MPS in NVs enhances the clearance of bacteria and inflammation resolution

We have successfully loaded both AZ and MPS in single Chol-NVs

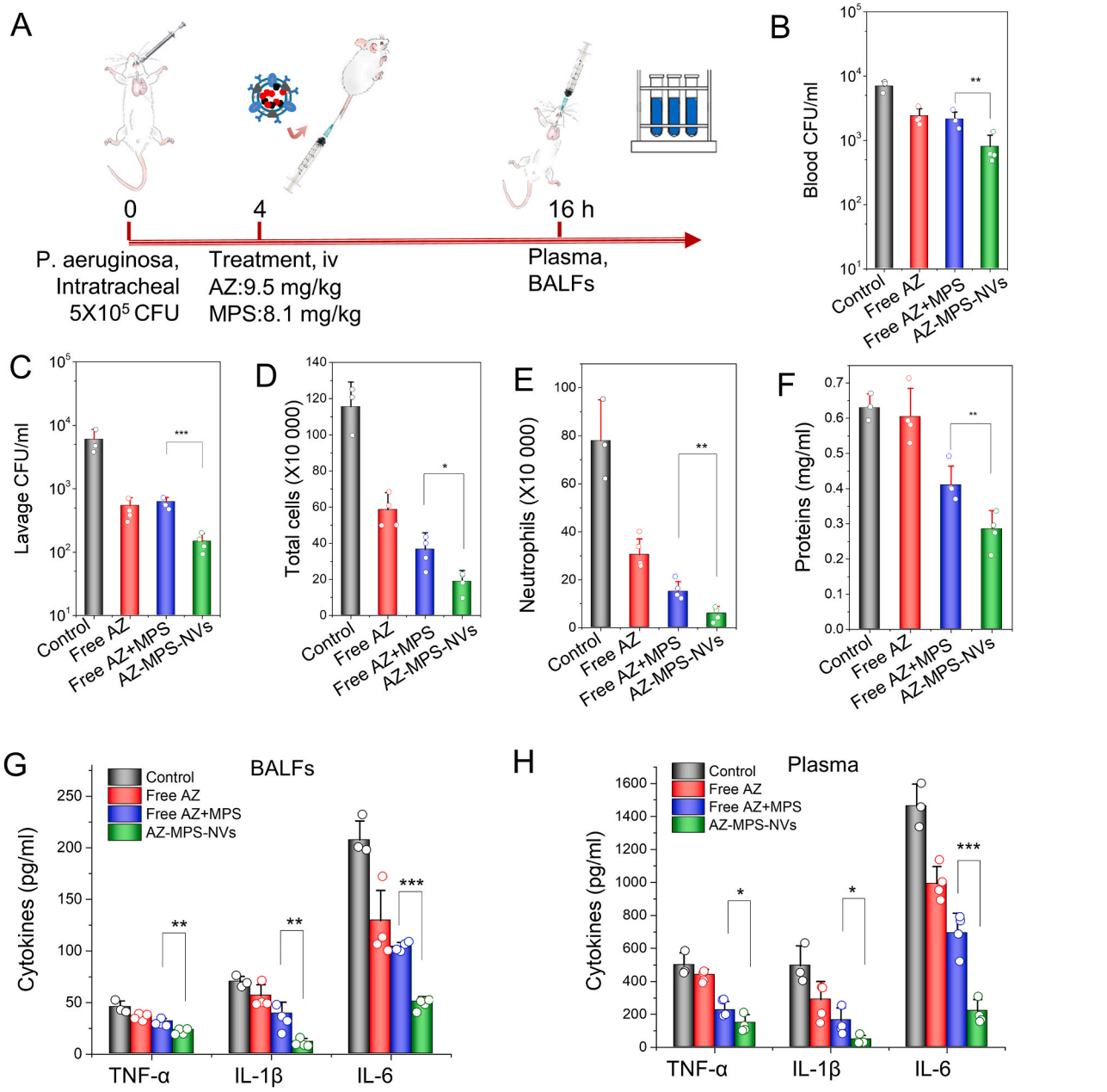

Fig. 7. Co-loading of AZ and MPS to NVs ameliorates bacterial burden and inflammation-induced lung damage in a mouse lung infection model. (A) Animal protocol for evaluating the therapeutic effect of AZ-MPS-NVs in the lung infection. CFU of bacteria in blood (B) and in the lung (C). Leukocytes (D) and neutrophils (E) in BALF; (F) the lung permeability determined by total proteins in BALF. Cytokines in BALF (G) and in blood (H). Data presented as the mean ± SD, n = 3,4. *P < 0.05, **P < 0.01, and ***P < 0.001.

and there are the high loading efficiencies in NVs (Fig. 6). We asked whether delivery of both AZ and MPS using NVs improve the therapy of bacterial infections. Therefore, we established a local lung infection animal model induced by *P. aeruginosa*. The lung infection was produced by intratracheal administration of 5×10^5 CFU *P. aeruginosa* in the mouse lung. 4 h later, the mice were treated with different formulations and 12 h after the administration of drugs, the blood and BALF were collected for evaluation of therapeutic effects (Fig. 7A). The results showed that the CFU counts of bacteria in circulation (Fig. 7B) and BALFs (Fig. 7C) were dramatically decreased when the mice were treated with AZ/MPS-loaded NVs compared to free drug formulations. Interestingly, we observed that only AZ can clear the bacteria rather than MPS when we compared free AZ to free AZ/MPS, suggesting that MPS (anti-inflammatory agent) did not affect the bacterial killing.

Furthermore, we analyzed the leukocyte lung infiltration, finding that AZ-MPS-NVs prevented leukocyte infiltration compared to free drug formulations (Fig. 7D), and the decrease of leukocyte infiltration came from neutrophils (Fig. 7E). The lung permeability is a hallmark of lung damage after bacterial infections [8]. The measurement of total proteins in BALF showed that AZ-MPS-NVs decreased the protein contents in the lung compared to other formulations (Fig. 7F), indicating that the inflammation was resolved to repair the lung edema. We also quantitatively measured cytokines (TNF-a, IL-1b and IL-6) in blood and the lung. Cytokines in BALF (Fig. 7G) and plasma (Fig. 7H) were decreased after treating mice with AZ-MPS-NVs compared to free drug formulations. Collectively, our data show that NVs increased the delivery of both AZ and MPS into the infectious lung, and AZ and MPS target the pathogens and inflammatory pathways, respectively. Therefore, AZ-MPS-NVs improve the therapeutic outcome of lung infection by *P. aeruginosa*.

Lung bacterial infections can cause the severe lung damage, such as ALI and ARDS, leading to the death. The molecular mechanisms of pathogenesis of ALI and ARDS are well-studied [8,55,56]. During lung infections, bacteria (such as *P. aeruginosa*) invade in the airspace of the lung and cause the host inflammation response. The lung vascular endothelium is activated to express intercellular adhesion molecules that recruit neutrophils into the lung. ALI or ARDS happens if inflammation response is out of control. Therefore, the invasion of pathogens and the host inflammation response are major targets to treat lung infections. However, specifically, and effectively delivering antibiotics and anti-inflammatory agents in the infectious lung is challenging because most these drugs do not have the tissue targeting ability.

In this paper, we proposed a novel strategy to effectively load both antibiotics and anti-inflammatory agents in single Chol-infilled NVs using pH gradient, and NVs can home to inflammatory vasculature because NVs possess vascular targeting ligands of their parent neutrophil membrane. We discovered that adding of cholesterol into the lipid bilayer of NVs can increase the membrane integrity of NVs to produce a pH gradient between intra-vesicles and outer vesicles (Fig. 2). Interestingly, dissolving of cholesterol in pyridine enhances the infilling of cholesterol to NVs and avoids the aggregations of NVs and denature of targeting protein ligands on NVs compared to using chloroform [26]. The studies have shown that adding of cholesterol to NVs does not change the amount of cellular targeting proteins on NVs, and the binding of NVs to activated endothelium in the live mouse inflammatory model (Fig. 3). Surprisingly, adding of cholesterol to NVs increases the uptake of NVs in activated vasculature, thus possibly improving the drug delivery efficiency.

Initially, we loaded single drug of MPS into NVs via pH gradient, and the drug loading efficiency can be achieved to 15% (w/w) (Fig. 4). To target both pathogens and inflammatory pathways, using the same approach we have successfully loaded both AZ and MPS into single NVs. We found that the maximum loading efficiency of AZ and MPS can be 19% (w/w) and 15% (w/w) (Fig. 6). Compared to single drug of MPS loaded to NVs, we found that individual drug loading does not interfere each other. In addition, we can reach the drug loading of AZ and MPS to be more than 30% (w/w), which could impact the translation of our remote loading technology. Finally, we tested our co-loading of AZ and MPS to NVs in the lung infection mouse model. We found that this novel formulation mitigated the inflammatory response and accelerated the bacterial clearance in the lung. Most interestingly, we observed that this novel formulation can accelerate the inflammation resolution to prevent the lung damage.

4. Conclusion

In summary, we demonstrate that infilling of cholesterol into the membrane of nanovesicles is a novel strategy to build the pH gradient between intra and outer-vesicles for remote drug loading. We can load single or multiple drugs into single nanovesicles, and the loading efficiency could be more than 30% (w/w). We also discover that adding of cholesterol in NVs enhances vasculature targeting because cholesterol increases the stiffness of NVs to facilitate the binding affinity of NVs to vasculature. In the lung infection mouse model, we have shown that co-loading of antibiotics and anti-inflammatory agents in NVs accelerates the bacterial clearance and inflammation resolution, thus preventing the potential of lung damage to lead to ARDS. Remote loading in liposomes has been successful to translate them to treat a wide range of diseases, such as vascular diseases and cancer. However, liposomal formulations lack of tissue targeting, thus decreasing the drug delivery efficiency. Our nanovesicles are biomimetic drug delivery platform to selectively target infectious sites, thus we expect the combination of remote loading of multiple drugs and our nanovesicle platform would be in a good position to translate our technology and approach in the future.

Credit author statement

Conceptualization, Z. W. and J. G.; Methodology, J. G and Y. S.; Investigation, J. G. and Y. S.; Writing – Original Draft, J. G. and Z. W; Editing, J. G. and Z. W.; Supervision, Z. W.; Funding Acquisition, Z. W.; All authors read and approved the final manuscript.

Declaration of competing interest

The authors declare that they have no known competing financial interests or personal relationships that could have appeared to influence the work reported in this paper.

Data availability

Data will be made available on request.

Acknowledgments

This work was financially supported by NIH grant R01EB027078 to Z. W.

Appendix A. Supplementary data

Supplementary data to this article can be found online at https://doi.org/10.1016/j.biomaterials.2023.122071.

References

[1] A. Morand, J.J. Morand, Pseudomonas aeruginosa in dermatology, Ann. Dermatol. Venereol. 144 (11) (2017) 666–675.
[2] C.H. Lee, T.Y. Su, J.J. Ye, P.C. Hsu, A.J. Kuo, J.H. Chia, M.H. Lee, Risk factors and clinical significance of bacteremia caused by Pseudomonas aeruginosa resistant only to carbapenems, Journal of microbiology, immunology, and infection = Wei mian yu gan ran za zhi 50 (5) (2017) 677–683.
[3] Y. Carmeli, J. Armstrong, P.J. Laud, P. Newell, G. Stone, A. Wardman, L.B. Gasink, Ceftazidime-avibactam or best available therapy in patients with ceftazidime-resistant Enterobacteriaceae and Pseudomonas aeruginosa complicated urinary tract infections or complicated intra-abdominal infections (REPRISE): a randomised, pathogen-directed, phase 3 study, the Lancet, Infectious diseases 16 (6) (2016) 661–673.
[4] K.A. Mielko, S.J. Jablonski, J. Milczewska, D. Sands, M. Lukaszewicz, P. Mlynarz, Metabolomic studies of Pseudomonas aeruginosa, World J. Microbiol. Biotechnol. 35 (11) (2019) 178.
[5] S. Wang, J. Gao, M. Li, L. Wang, Z. Wang, A facile approach for development of a vaccine made of bacterial double-layered membrane vesicles (DMVs), Biomaterials 187 (2018) 28–38.
[6] R.T. Sadikot, H. Zeng, M. Joo, M.B. Everhart, T.P. Sherrill, B. Li, D.S. Cheng, F. E. Yull, J.W. Christman, T.S. Blackwell, Targeted immunomodulation of the NF-kappaB pathway in airway epithelium impacts host defense against Pseudomonas aeruginosa, J. Immunol. 176 (8) (2006) 4923–4930.
[7] J.P. Mizgerd, Respiratory infection and the impact of pulmonary immunity on lung health and disease, Am. J. Respir. Crit. Care Med. 186 (9) (2012) 824–829.
[8] M.A. Matthay, L.B. Ware, G.A. Zimmerman, The acute respiratory distress syndrome, J. Clin. Invest. 122 (8) (2012) 2731–2740.
[9] M.A. Matthay, R.L. Zemans, The acute respiratory distress syndrome: pathogenesis and treatment, Annu. Rev. Pathol. 6 (2011) 147–163.
[10] L.B. Ware, M.A. Matthay, Clinical practice. Acute pulmonary edema, N. Engl. J. Med. 353 (26) (2005) 2788–2796.
[11] B.T. Thompson, R.C. Chambers, K.D. Liu, Acute respiratory distress syndrome, N. Engl. J. Med. 377 (6) (2017) 562–572.
[12] L.S.J. Roope, R.D. Smith, K.B. Pouwels, J. Buchanan, L. Abel, P. Eibich, C.C. Butler, P.S. Tan, A.S. Walker, J.V. Robotham, S. Wordsworth, The challenge of antimicrobial resistance: what economics can contribute, Science 364 (6435) (2019).
[13] F.M. Aarestrup, J. Engberg, Antimicrobial resistance of thermophilic Campylobacter, Vet. Res. 32 (3–4) (2001) 311–321.
[14] N. Kashef, M.R. Hamblin, Can microbial cells develop resistance to oxidative stress in antimicrobial photodynamic inactivation? Drug Resist. Updates 31 (2017) 31–42.
[15] J. Gao, Y. Su, Z. Wang, Engineering bacterial membrane nanovesicles for improved therapies in infectious diseases and cancer, Adv. Drug Deliv. Rev. 186 (2022), 114340.
[16] X.Y. Dong, C.Y. Zhang, J. Gao, Z.J. Wang, Targeting of nanotherapeutics to infection sites for antimicrobial therapy, Adv Ther-Germany 2 (11) (2019).
[17] C.Y. Zhang, J. Gao, Z. Wang, Bioresponsive nanoparticles targeted to infectious microenvironments for sepsis management, Adv. Mater. 30 (43) (2018), e1803618.

[18] J. Gao, D. Chu, Z. Wang, Cell membrane-formed nanovesicles for disease-targeted delivery, J. Contr. Release 224 (2016) 208–216.
[19] J. Gao, X. Dong, Y. Su, Z. Wang, Human neutrophil membrane-derived nanovesicles as a drug delivery platform for improved therapy of infectious diseases, Acta Biomater. 123 (2021) 354–363.
[20] J. Gao, S. Wang, Z. Wang, High yield, scalable and remotely drug-loaded neutrophil-derived extracellular vesicles (EVs) for anti-inflammation therapy, Biomaterials 135 (2017) 62–73.
[21] J. Gao, S. Wang, X. Dong, L.G. Leanse, T. Dai, Z. Wang, Co-delivery of resolvin D1 and antibiotics with nanovesicles to lungs resolves inflammation and clears bacteria in mice, Commun Biol 3 (1) (2020) 680.
[22] J. Gao, M. Lee, X. Dong, Z. Wang, Generation of membrane-derived nanovesicles by nitrogen cavitation for drug targeting delivery and immunization, Methods Mol. Biol. 2394 (2022) 575–589.
[23] S. Malhotra, S. Dumoga, A. Joshi, S. Mohanty, N. Singh, Polymeric micelles coated with hybrid nanovesicles enhance the therapeutic potential of the reversible topoisomerase inhibitor camptothecin in a mouse model, Acta Biomater. 121 (2021) 579–591.
[24] Y. Chu, J. Zhang, H. Pan, J. Shi, J. Wang, L. Chen, Preparation and evaluation of long circulating erythrocyte membrane-cloaked anti-cancer drug delivery system, Drug Deliv Transl Res 10 (5) (2020) 1278–1287.
[25] R.H. Fang, A.V. Kroll, W. Gao, L. Zhang, Cell membrane coating nanotechnology, Adv. Mater. 30 (23) (2018), e1706759.
[26] X. Zhang, P. Angsantikul, M. Ying, J. Zhuang, Q. Zhang, X. Wei, Y. Jiang, Y. Zhang, D. Dehaini, M. Chen, Y. Chen, W. Gao, R.H. Fang, L. Zhang, Remote loading of small-molecule therapeutics into cholesterol-enriched cell-membrane-derived vesicles, Angew Chem. Int. Ed. Engl. 56 (45) (2017) 14075–14079.
[27] T.M. Allen, P.R. Cullis, Liposomal drug delivery systems: from concept to clinical applications, Adv. Drug Deliv. Rev. 65 (1) (2013) 36–48.
[28] D. Zucker, D. Marcus, Y. Barenholz, A. Goldblum, Liposome drugs' loading efficiency: a working model based on loading conditions and drug's physicochemical properties, J. Contr. Release 139 (1) (2009) 73–80.
[29] Y. Barenholz, Doxil(R)–the first FDA-approved nano-drug: lessons learned, J. Contr. Release 160 (2) (2012) 117–134.
[30] C.D. Pritchard, T.M. O'Shea, D.J. Siegwart, E. Calo, D.G. Anderson, F.M. Reynolds, J.A. Thomas, J.R. Slotkin, E.J. Woodard, R. Langer, An injectable thiol-acrylate poly(ethylene glycol) hydrogel for sustained release of methylprednisolone sodium succinate, Biomaterials 32 (2) (2011) 587–597.
[31] S. Altamentova, P. Rumajogee, J. Hong, S.R. Beldick, S.J. Park, A. Yee, M. G. Fehlings, Methylprednisolone reduces persistent post-ischemic inflammation in a rat hypoxia-ischemia model of perinatal stroke, Transl Stroke Res 11 (5) (2020) 1117–1136.
[32] G.L. Drusano, S.C. Schimpff, W.L. Hewitt, The acylampicillins: mezlocillin, piperacillin, and azlocillin, Rev. Infect. Dis. 6 (1) (1984) 13–32.
[33] A. Alizadeh, M. Salouti, H. Alizadeh, A.R. Kazemizadeh, A.A. Safari, S. Mahmazi, Enhanced antibacterial effect of azlocillin in conjugation with silver nanoparticles against Pseudomonas aeruginosa, IET Nanobiotechnol. 11 (8) (2017) 942–947.
[34] J. Gao, S. Wang, X. Dong, Z. Wang, RGD-expressed bacterial membrane-derived nanovesicles enhance cancer therapy via multiple tumorous targeting, Theranostics 11 (7) (2021) 3301–3316.
[35] Z. Wang, J. Li, J. Cho, A.B. Malik, Prevention of vascular inflammation by nanoparticle targeting of adherent neutrophils, Nat. Nanotechnol. 9 (3) (2014) 204–210.
[36] J. Zhang, Q. Li, Y. Wu, D. Wang, L. Xu, Y. Zhang, S. Wang, T. Wang, F. Liu, M. Y. Zaky, S. Hou, S. Liu, K. Zou, H. Lei, L. Zou, Y. Zhang, H. Liu, Cholesterol content in cell membrane maintains surface levels of ErbB2 and confers a therapeutic vulnerability in ErbB2-positive breast cancer, Cell Commun. Signal. 17 (1) (2019) 15.
[37] H.A. Scheidt, T. Meyer, J. Nikolaus, D.J. Baek, I. Haralampiev, L. Thomas, R. Bittman, P. Muller, A. Herrmann, D. Huster, Cholesterol's aliphatic side chain modulates membrane properties, Angew. Chem. 52 (49) (2013) 12848–12851.
[38] H. Alobeedallah, B. Cornell, H. Coster, The effect of cholesterol on the voltage-current characteristics of tethered lipid membranes, J. Membr. Biol. 253 (4) (2020) 319–330.
[39] Z. Hong, I. Ersoy, M. Sun, F. Bunyak, P. Hampel, Z. Hong, Z. Sun, Z. Li, I. Levitan, G.A. Meininger, K. Palaniappan, Influence of membrane cholesterol and substrate elasticity on endothelial cell spreading behavior, J. Biomed. Mater. Res., Part A 101 (7) (2013) 1994–2004.
[40] A. Gorman, K.R. Hossain, F. Cornelius, R.J. Clarke, Penetration of phospholipid membranes by poly-l-lysine depends on cholesterol and phospholipid composition, Biochimica et biophysica acta, Biomembranes 1862 (2) (2020), 183128.
[41] D. Chu, J. Gao, Z. Wang, Neutrophil-Mediated delivery of therapeutic nanoparticles across blood vessel barrier for treatment of inflammation and infection, ACS Nano 9 (12) (2015) 11800–11811.
[42] X. Dong, D. Chu, Z. Wang, Leukocyte-mediated delivery of nanotherapeutics in inflammatory and tumor sites, Theranostics 7 (3) (2017) 751–763.
[43] D. Chu, X. Dong, X. Shi, C. Zhang, Z. Wang, Neutrophil-based drug delivery systems, Adv. Mater. 30 (22) (2018), e1706245.
[44] X. Dong, D. Chu, Z. Wang, Neutrophil-mediated delivery of nanotherapeutics across blood vessel barrier, Ther. Deliv. 9 (1) (2018) 29–35.
[45] C. Paslack, J.C. Smith, M. Heyden, L.V. Schafer, Hydration-mediated stiffening of collective membrane dynamics by cholesterol, Phys. Chem. Chem. Phys. : Phys. Chem. Chem. Phys. 21 (20) (2019) 10370–10376.
[46] K.N. Liu, S.G. Boxer, Target membrane cholesterol modulates single influenza virus membrane fusion efficiency but not rate, Biophys. J. 118 (10) (2020) 2426–2433.
[47] H. Oh, E.R. Mohler 3rd, A. Tian, T. Baumgart, S.L. Diamond, Membrane cholesterol is a biomechanical regulator of neutrophil adhesion, Arterioscler. Thromb. Vasc. Biol. 29 (9) (2009) 1290–1297.
[48] M. Acar, M. Gedizlioglu, A. Koskderelioglu, F. Ozturk, S. Kilinc, N. Talay, Effect of high-dose intravenous methyl-prednisolone treatment on intraocular pressure in multiple sclerosis patients with relapse, Eur. Neurol. 68 (1) (2012) 20–22.
[49] D. Franciotta, G. Piccolo, E. Zardini, R. Bergamaschi, V. Cosi, Soluble CD8 and ICAM-1 in serum and CSF of MS patients treated with 6-methylprednisolone, Acta Neurol. Scand. 95 (5) (1997) 275–279.
[50] T. Hagi, Y. Kurokawa, N. Kobayashi, T. Takahashi, T. Saito, K. Yamashita, K. Tanaka, T. Makino, M. Yamasaki, K. Nakajima, H. Eguchi, Y. Doki, Anti-metastatic effect of methylprednisolone targeting vascular endothelial cells under surgical stress, Sci. Rep. 11 (1) (2021) 6268.
[51] H. Zhang, Y. Park, J. Wu, X. Chen, S. Lee, J. Yang, K.C. Dellsperger, C. Zhang, Role of TNF-alpha in vascular dysfunction, Clin. Sci. (Lond.) 116 (3) (2009) 219–230.
[52] F. Mackay, H. Loetscher, D. Stueber, G. Gehr, W. Lesslauer, Tumor-necrosis-factor-Alpha (Tnf-Alpha)-Induced cell-adhesion to human endothelial-cells is under dominant control of one tnf receptor type, tnf-R55, J. Exp. Med. 177 (5) (1993) 1277–1286.
[53] M.A. Matthay, R.L. Zemans, G.A. Zimmerman, Y.M. Arabi, J.R. Beitler, A. Mercat, M. Herridge, A.G. Randolph, C.S. Calfee, Acute respiratory distress syndrome, Nat. Rev. Dis. Prim. 5 (1) (2019) 18.
[54] C.C. Sanders, Azlocillin: a new broad spectrum penicillin, J. Antimicrob. Chemother. 11 (Suppl B) (1983) 21–31.
[55] C.Y. Zhang, W. Lin, J. Gao, X. Shi, M. Davaritouchaee, A.E. Nielsen, R.J. Mancini, Z. Wang, pH-responsive nanoparticles targeted to lungs for improved therapy of acute lung inflammation/injury, ACS Appl. Mater. Interfaces 11 (18) (2019) 16380–16390.
[56] C.Y. Zhang, X. Dong, J. Gao, W. Lin, Z. Liu, Z. Wang, Nanoparticle-induced neutrophil apoptosis increases survival in sepsis and alleviates neurological damage in stroke, Sci. Adv. 5 (11) (2019), eaax7964.